UC Berkeley
UC Berkeley Previously Published Works

Title
Co-Occurring Weather Systems Vary by Atmospheric River Scale Across the United States

Permalink
https://escholarship.org/uc/item/84z6354k

Journal
Geophysical Research Letters, 53(18)

ISSN
0094-8276

Authors
Kamnani, Diya
O'Brien, Travis A
Tsai, Wei-Ming
et al.

Publication Date
2026-09-28

DOI
10.1029/2026gl123975

Copyright Information
This work is made available under the terms of a Creative Commons Attribution License, available at https://creativecommons.org/licenses/by/4.0/

Peer reviewed

eScholarship.org Powered by the California Digital Library
University of California

Check for updates

Geophysical Research Letters

RESEARCH LETTER
10.1029/2026GL123975

Co-Occurring Weather Systems Vary by Atmospheric River Scale Across the United States

Diya Kamnani[1], Travis A. O'Brien[1,2], Wei-Ming Tsai[3], Kwesi Twentwewa Quagraine[4], J. David Neelin[3], Jennifer L. Catto[5], Yang Zhou[2], L. Ruby Leung[6], William R. Boos[2,7], and Hongsheng Wang[5]

[1]Department of Earth and Atmospheric Sciences, Indiana University, Bloomington, IN, USA, [2]Climate and Ecosystem Sciences Division, Lawrence Berkeley National Laboratory, Berkeley, CA, USA, [3]Department of Atmospheric and Oceanic Sciences, University of California, Los Angeles, Los Angeles, CA, USA, [4]Department of Atmospheric Sciences, Texas A&M University, College Station, TX, USA, [5]Department of Mathematics and Statistics, University of Exeter, Exeter, UK, [6]Atmospheric, Climate, and Earth Sciences Division, Pacific Northwest National Laboratory, Richland, WA, USA, [7]Department of Earth and Planetary Science, University of California, Berkeley, Berkeley, CA, USA

Key Points:

- AR + Front combinations dominate across much of the conterminous U.S., while Gulf and offshore Pacific regions show greater complexity
- In DJF and MAM, higher AR scales more often co-occur with fronts and MCSs; in JJA and SON, additional LPS co-occurrence becomes evident
- Each season has different mixtures of weather phenomena associated with extreme precipitation

Supporting Information:

Supporting Information may be found in the online version of this article.

Correspondence to:

D. Kamnani,
dkamnani@iu.edu

Citation:

Kamnani, D., O'Brien, T. A., Tsai, W.-M., Quagraine, K. T., Neelin, J. D., Catto, J. L., et al. (2026). Co-occurring weather systems vary by atmospheric river scale across the United States. *Geophysical Research Letters*, *53*, e2026GL123975. https://doi.org/10.1029/2026GL123975

Received 26 APR 2026
Accepted 18 AUG 2026

Abstract Atmospheric Rivers (ARs) often co-occur with other weather systems, including fronts, low-pressure systems (LPSs), and mesoscale convective systems (MCSs), which can amplify precipitation and flood risk. While extreme rainfall is frequently linked to multiple interacting features, how these systems co-occur with AR intensity scales and regions remains unclear. Using ERA5-derived feature masks and satellite data, we quantify spatiotemporal overlaps between ARs and other systems. AR + Front combinations dominate across much of the conterminous U.S. In higher AR scales (4–5), more complex MCS-related combinations become increasingly common, particularly in DJF and MAM and along the West Coast, while limited LPS-related co-occurrences appear mainly in JJA and SON and are confined to regions such as the Gulf of Mexico and offshore Pacific genesis regions. In contrast, AR-only occurrences dominate in some inland western regions. Extreme precipitation exhibits seasonal variation, with distinct co-occurring systems contributing across seasons.

Plain Language Summary Atmospheric Rivers (ARs) transport large amounts of moisture and are major contributors to heavy rainfall and flooding. ARs often occur alongside other weather systems, such as fronts, low-pressure systems (LPSs), and mesoscale convective systems (MCSs), which can influence where and when heavy rainfall occurs. Here, we examine how ARs overlap with these systems across different AR intensity scales and regions. Our results show that AR–Front interactions are most common across much of the United States. Higher AR scales are more likely to co-occur with MCSs and, in some regions, LPSs as well, particularly during summer and autumn and near the Gulf of Mexico and offshore Pacific genesis regions. The patterns of overlapping weather systems change with the seasons, and stronger ARs often occur alongside more overlapping systems.

1. Introduction

Atmospheric River (AR) events pose significant risks to the U.S. economy through flood damage, with estimated annual losses exceeding $1 billion in the western United States alone (Corringham et al., 2019). ARs are a dominant driver of extreme precipitation across the continental U.S., transporting vast amounts of moisture into the midlatitudes and frequently interacting with other weather systems, including frontal systems, mesoscale convective systems (MCSs), and low-pressure systems (LPSs) (Gimeno et al., 2020; Tsai et al., 2025). AR moisture sources have been linked to convergence along trailing cold fronts, underscoring the well-known dynamical connection between ARs and frontal systems (Bao et al., 2006; Newell & Zhu, 1994; Prein et al., 2023). Case studies over the central U.S. demonstrate that ARs can support the development of MCSs by providing favorable available potential energy (Moore et al., 2012; O'Brien et al., 2024). In addition, tropical cyclones can act as significant moisture sources for ARs, with case studies demonstrating the development of AR-like moisture plumes linked to tropical cyclone outflow and subsequent interaction with midlatitude systems (Cordeira et al., 2013). Collectively, these examples demonstrate that ARs can co-occur with varied weather phenomena to produce flooding and extreme precipitation across the U.S. (Hsu & Chen, 2020; Mahoney et al., 2016; Neiman et al., 2008), highlighting the importance of understanding these interactions.

© 2026. Battelle Memorial Institute, Lawrence Berkeley National Laboratory and The Author(s). This article has been contributed to by U.S. Government employees and their work is in the public domain in the USA.
This is an open access article under the terms of the Creative Commons Attribution License, which permits use, distribution and reproduction in any medium, provided the original work is properly cited.

19448007, 2026, 18, Downloaded from https://agupubs.onlinelibrary.wiley.com/doi/10.1029/2026GL123975, Wiley Online Library on [03/11/2026]. See the Terms and Conditions (https://onlinelibrary.wiley.com/terms-and-conditions) on Wiley Online Library for rules of use; OA articles are governed by the applicable Creative Commons License

Understanding patterns of AR co-occurrence is therefore critical for improving preparedness, mitigating risks, and better understanding the drivers of extreme precipitation across regions. Prior studies indicate that extreme precipitation often results from interactions among multiple weather systems (Catto & Dowdy, 2021), with the dominant interactions varying by event intensity (Prein et al., 2023) and region. For example, Tsai et al. (2025) finds that AR-Front co-occurrences account for a large fraction of precipitation in the extratropics, whereas MCS-LPS interactions dominate in the tropics. These findings highlight that while multiple systems can jointly produce extreme precipitation, ARs remain a particularly important driver of flooding across the continental U.S (Corringham et al., 2019; Lavers & Villarini, 2013; Pradhan et al., 2026).

Building on this understanding, we hypothesize that AR co-occurrence with other weather systems varies systematically by AR scale and region, with higher AR scales involving a greater number of interacting phenomena. AR scale, defined by integrated vapor transport (IVT) and duration at a given location (Ralph et al., 2019), is widely used as an indicator of likely precipitation intensity, flood severity, and associated economic losses, with higher AR scales corresponding to greater impacts (Corringham et al., 2019). Here, we use this scale-based framework to investigate which types of co-occurrence dominate across different regions of the continental U.S. and how these patterns influence extreme precipitation potential.

2. Data and Methodology

2.1. Data

This study uses a published data set of objectively identified atmospheric features, including ARs, fronts, MCSs, and tropical-subtropical LPSs, developed and described in Tsai et al. (2025). The data set spans 19 years (2001–2019) and is provided on the ERA5 reanalysis grid (Hersbach et al., 2020), with atmospheric fields at 0.25° horizontal resolution. The published data set is available at 6-hourly intervals, consistent with the availability of front detections and aligned across all feature types. The analysis domain encompasses the continental United States (CONUS), extending from 0°N to 60°N and from 50°W to 160°W. LPS detections are limited to south of 35°N and therefore only partially cover the full analysis domain.

ARs are identified using the TECA_BARD algorithm, a Bayesian-based detection framework (O'Brien et al., 2022). Fronts are identified using an objective gradient-based detection algorithm (Sansom & Catto, 2024), without considering front type. MCSs are tracked using the FLEXible object TRacKeR (FLEXTRKR), which combines satellite-derived cold cloud shields with precipitation features to identify and track robust convective systems lasting longer than 4 hr (Feng et al., 2023). LPSs are identified using the TempestExtremes feature tracker applied to the 850 hPa streamfunction field (Vishnu et al., 2020). Precipitation is evaluated using the GPM IMERG V6 data set (Huffman et al., 2015), along with the Climate Prediction Center (CPC) merged infrared data set (Janowiak et al., 2001), used for consistency with MCS tracking. Details on individual methodologies as well as the combined data set are described in Tsai et al. (2025) and references therein. We use the provided feature masks directly without modification.

As multiple detection methods exist for ARs, fronts, MCSs, and LPSs, the identified patterns may vary depending on the algorithms and thresholds employed. Given the focus on AR events in this study, AR detection represents an important source of uncertainty, as different AR detection tools can produce different feature extents. However, intercomparison studies have shown that AR detection methods generally capture similar large-scale meteorological phenomena despite differences in their identified boundaries (K. T. Quagraine et al., 2025). Additional uncertainties arise from precipitation attribution, as the finite boundaries of identified features may not capture the full spatial extent of associated precipitation. While these factors may influence quantitative estimates, they are less likely to affect the broader seasonal and regional patterns emphasized here; further discussion is provided in Tsai et al. (2025) and the Supplement.

2.2. Methodology

Analyses are conducted on a common gridcell basis to examine AR occurrence across scales, co-occurrence with other weather systems, and associated precipitation. Results are evaluated across the domain for the annual mean and the four standard seasons (DJF, MAM, JJA, SON) to capture seasonal contrasts in AR events.

We categorize AR events following the AR scale established by Ralph et al. (2019), which classifies events based on IVT magnitude and duration at each grid cell. Scales are assigned using the ARCat Python package

19448007, 2026, 18, Downloaded from https://agupubs.onlinelibrary.wiley.com/doi/10.1029/2026GL123975, Wiley Online Library on [03/11/2026]. See the Terms and Conditions (https://onlinelibrary.wiley.com/terms-and-conditions) on Wiley Online Library for rules of use; OA articles are governed by the applicable Creative Commons License

(K. Quagraine, 2024), which provides AR scale information across the 19-year record. We refer the reader to Ralph et al. (2019) for a detailed description of the full categorization scheme.

Building on this framework, we next quantify the co-occurrence of ARs with other meteorological phenomena using the identified feature masks. AR occurrence is identified using the binary AR mask from TECA_BARD algorithm. For selected events, we quantify co-occurrence by identifying all grid cells and time steps where ARs overlap with other phenomena, including fronts, MCSs, and LPSs, based on their respective masks. For each AR scale and grid cell, the frequency of each co-occurring feature combination is computed as the fraction of time steps with AR occurrence that are associated with that combination. These frequencies are aggregated spatially to yield annual and seasonal percentage contribution of each co-occurring system combination to total AR activity at each AR scale. The dominant co-occurring system for a given AR scale is defined as the co-occurrence combination with the highest frequency, while the second dominant system corresponds to the second-highest frequency combination for the particular gridcell.

Precipitation is also analyzed at the grid cell level and stratified by season, AR scale, and co-occurring system. For each AR scale, we compute the fractional contribution of precipitation from different co-occurring systems, expressed as a percentage of total precipitation during AR conditions. This quantifies how different feature combinations contribute to overall AR-related precipitation.

To focus on high-impact events, we repeat this analysis for nonzero precipitation exceeding the 90th percentile at each grid cell, where the percentile is computed over the full 19-year record. For these extreme events, we compute the fractional contribution of each co-occurring feature to total extreme precipitation, allowing us to assess how extreme rainfall associated with different AR scales changes in co-occurring systems.

The authors also acknowledge the use of AI-powered tools, including OpenAI's ChatGPT, for assistance with code development and language refinement during manuscript preparation.

3. Results

3.1. Case Studies of Co-Occurring Phenomena in ARs

We use two AR scale 5 case studies (Figure 1), one over the west coast of the U.S. and the other over the southeastern U.S., to illustrate the co-occurrence of different weather phenomena (MCS, LPS, and fronts) to AR events.

In Figure 1a, 500-hPa height contours remain largely parallel along the AR, with closely spaced contours in the tail region indicating a strong pressure gradient and concentrated moisture transport, and broader spacing toward the leading edge as the flow spreads, consistent with the previous studies (Bjerknes & Solberg, 1922; H. Dacre, 2020). Figure 1c shows the West Coast AR dominated by AR + Front + MCS. AR + Front is the next most prevalent combination, while AR-only (∼5%) and AR + MCS (∼2.5%) remain minor. This structure is characteristic of a "classic" extratropical cyclone-associated AR, where alignment with the low-level jet and warm conveyor belt favors moisture transport and co-occurrence with frontal systems and embedded convection (Bao et al., 2006; Neiman et al., 2008; Ralph et al., 2004, 2005, 2006; Wernli & Davies, 1997; Zhang et al., 2019).

In Figure 1b, a ridge (∼5,925 m) over the southeastern U.S., around which the AR curves. North of the AR, contours remain parallel, indicating organized mid-level flow that channels moisture along the AR axis. This event is associated with Tropical Cyclone Bill, which produced over 30 cm of rainfall in some regions during 16–21 June (Wakefield et al., 2021). Figure 1d shows that AR-only pixels are most prevalent, AR + LPS, while AR + MCS + LPS and AR + Front each account for 13%. Unlike the West Coast case, this event is more strongly linked to Tropical Cyclone Bill, whose circulation transported Gulf of Mexico moisture inland and supported enhanced convection, as confirmed by back-trajectory and radar analyses (Wakefield et al., 2021).

These contrasting cases demonstrate that ARs of the same scale can arise from different combinations of co-occurring systems. To assess how systematic these differences are, we next examine co-occurrence patterns across the CONUS and their seasonal variability.

3.2. AR Co-Occurrence Pattern Across Seasons and Scales

Figure 2 illustrates how the relative prevalence of different co-occurring weather systems within precipitating pixels changes with AR scale on annual and seasonal timescales. In Figure 2a, higher AR scales exhibit a greater

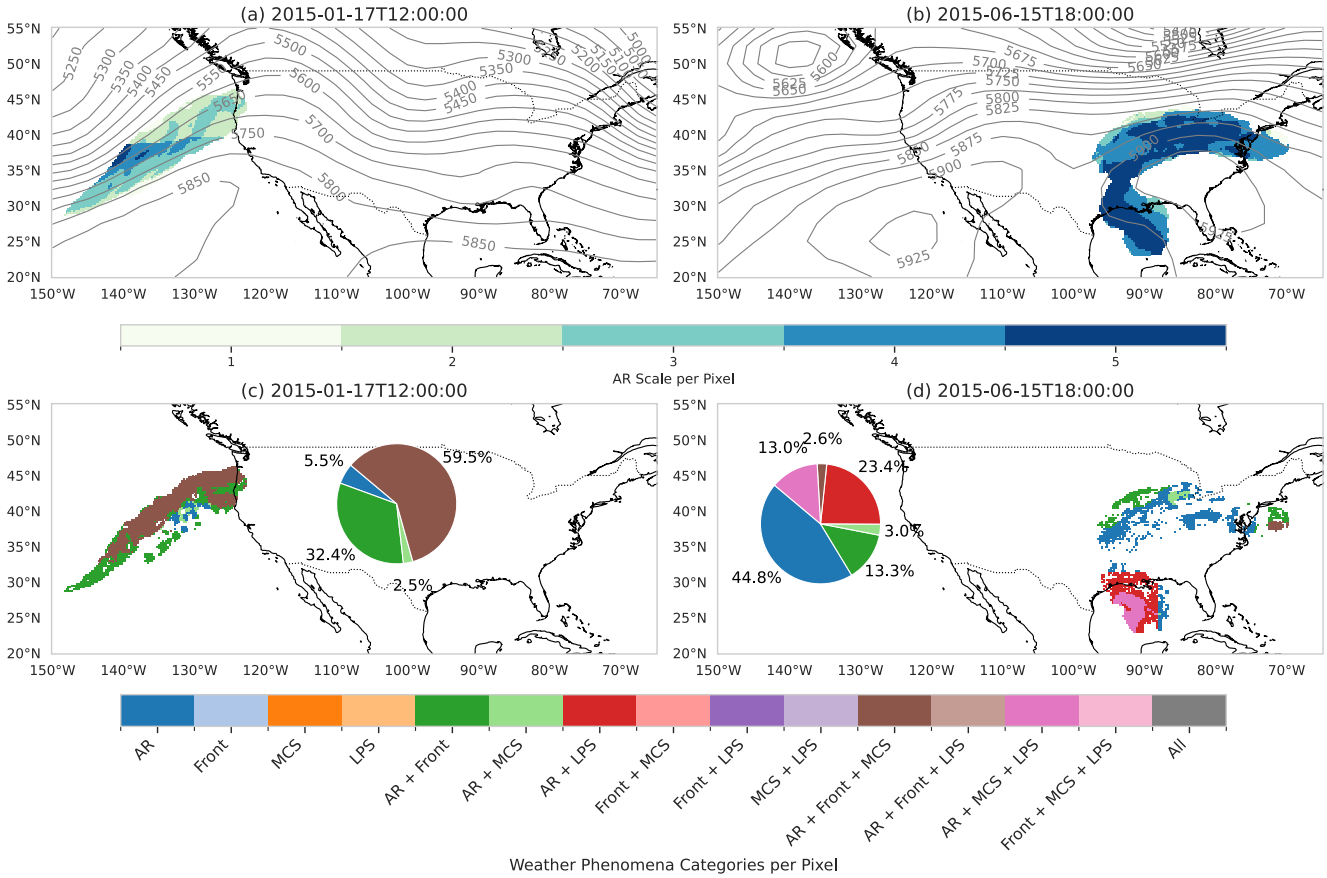


Figure 1. Two case studies illustrating the contribution of different weather phenomena to individual AR events. (a) and (b) show AR scales on two different days, with colors representing the AR scale for each pixel. The 500 hPa geopotential height contours (gray dashed lines) are overlaid to illustrate large-scale flow patterns associated with each AR. (c) and (d) display the corresponding co-occurring weather phenomena associated with precipitation within the AR footprint. The pie charts summarize the fractional co-occurrence of each phenomenon to the total AR area.

diversity of co-occurring feature combinations in the upper portions of the stacked bars, suggesting that stronger ARs are associated with more complex overlapping phenomena. When broken down by season, AR + Front is the dominant co-occurrence combination across all seasons and AR scales (Figures 2b–2e). DJF (Figure 2b) exhibits a higher prevalence of AR + Front + MCS than other seasons, particularly in the higher AR scales, indicating a stronger influence of extratropical cyclone-associated environments and organized convection during winter. MAM (Figure 2c) shows a stronger dominance of AR + Front across most scales, while AR + Front + MCS is less prevalent than in DJF but becomes more prominent in AR scale 5. These patterns are consistent with the stronger cool-season association between ARs and extratropical cyclones, when ARs are frequently embedded within strong pressure-gradient environments and frontal systems that can support mesoscale convection (Bao et al., 2006; Neiman et al., 2008; Ralph et al., 2004; Zhang et al., 2019).

In JJA and SON (Figures 2d and 2e), although AR + Front remains the most prevalent combination, LPS-related events become more discernible in the strongest AR scales, particularly in SON. JJA has the highest AR-only prevalence (>20%), while AR + Front + MCS is least prevalent across all AR scales compared to other seasons. In SON, AR + Front + MCS is slightly more prevalent than in JJA. Both seasons also exhibit increased LPS-related combinations, such as AR + LPS and AR + MCS + LPS, especially in AR scale 5, though these remain below 10%. These patterns may reflect greater interaction between ARs and LPS-related systems during summer and autumn, potentially supported by enhanced low-level moisture availability from the Gulf of Mexico and the tropical Atlantic. The Atlantic hurricane season (June–November) overlaps with this period and may contribute to increased LPS occurrence through tropical storms and hurricanes (Landsea, 1993). Additionally, stronger meridional moisture transport associated with low-level jets, such as the Great Plains low-level jet, may

19448007, 2026, 18, Downloaded from https://agupubs.onlinelibrary.wiley.com/doi/10.1029/2026GL123975, Wiley Online Library on [03/11/2026]. See the Terms and Conditions (https://onlinelibrary.wiley.com/terms-and-conditions) on Wiley Online Library for rules of use; OA articles are governed by the applicable Creative Commons License

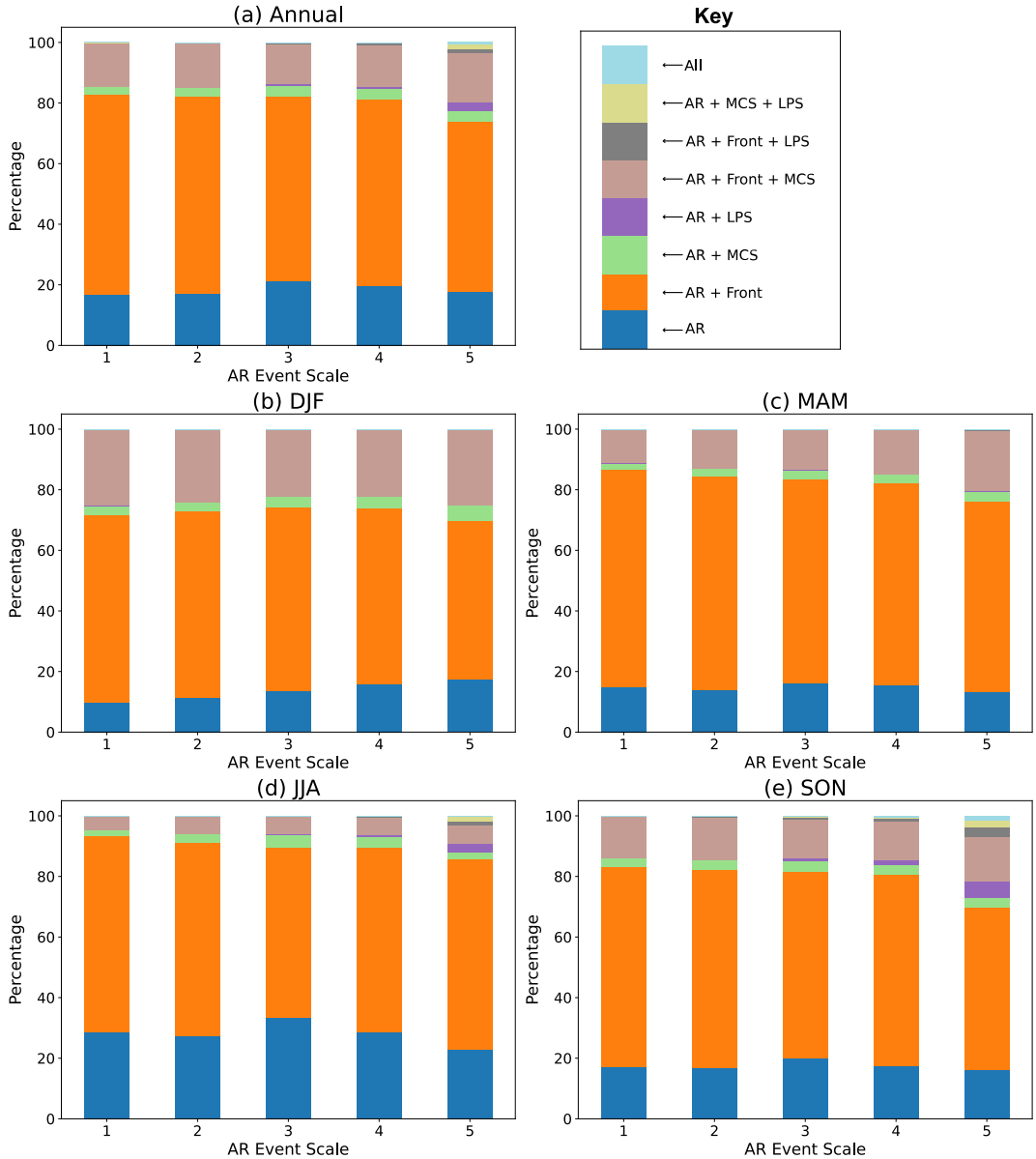


Figure 2. Relative contribution of different weather systems and their co-occurrences to AR-related precipitation across annual and seasonal scales. Each stacked bar represents the fraction of precipitating grid cells associated with each co-occurrence type when an AR is present. (a) Shows the annual distribution, while (b–e) represent the seasonal distributions for DJF, MAM, JJA, and SON, respectively.

channel moisture northward and promote interactions between ARs and other synoptic and mesoscale systems (Algarra et al., 2019; Gimeno et al., 2016).

These results support the contrasting archetypes illustrated in Figure 1. Front-associated ARs represent the dominant regime across all seasons and AR scales. In DJF and MAM, higher AR scales exhibit enhanced mesoscale convective co-occurrence, while in JJA and SON, higher AR scales exhibit additional complexity through the emergence of both MCS- and LPS-related co-occurrences. The following section examines where these different AR types are most likely to occur.

19448007, 2026, 18, Downloaded from https://agupubs.onlinelibrary.wiley.com/doi/10.1029/2026GL123975, Wiley Online Library on [03/11/2026]. See the Terms and Conditions (https://onlinelibrary.wiley.com/terms-and-conditions) on Wiley Online Library for rules of use; OA articles are governed by the applicable Creative Commons License

10.1029/2026GL123975

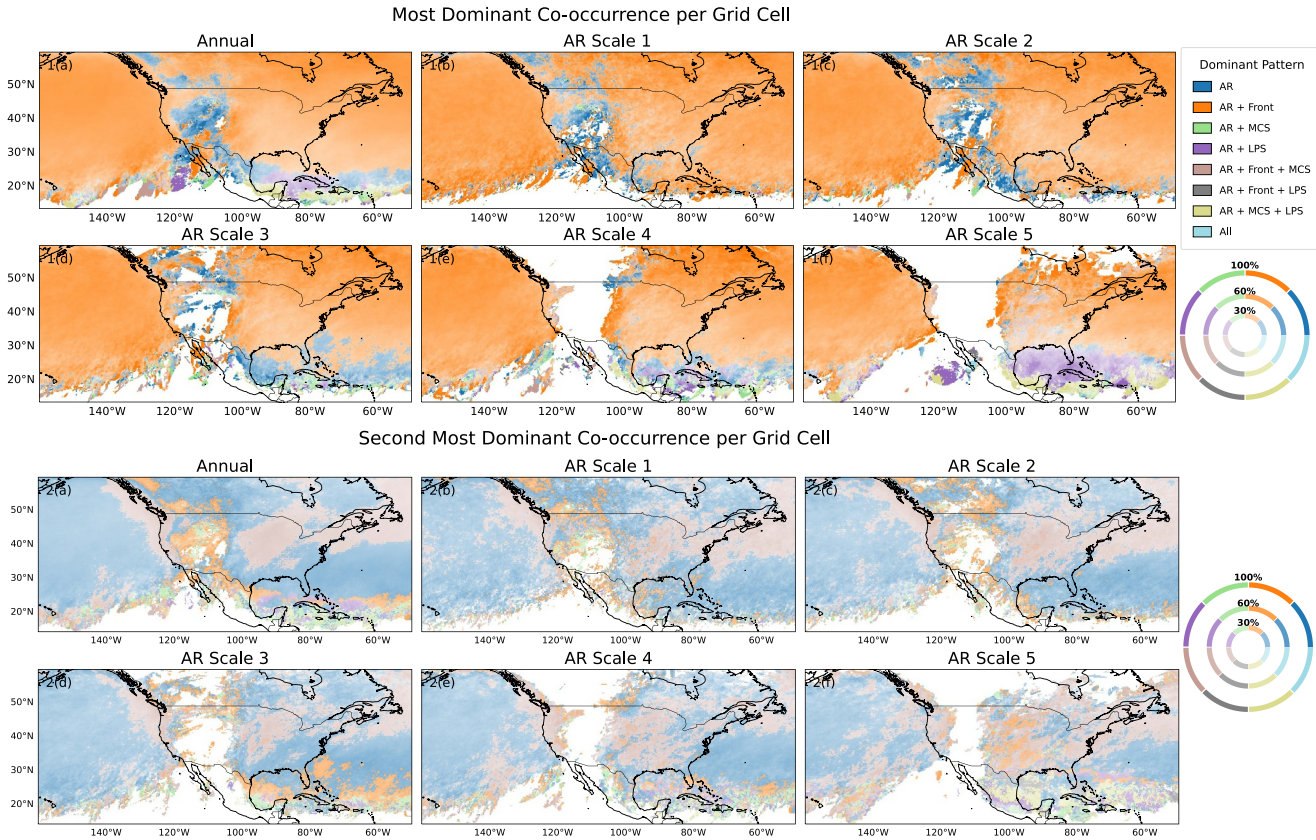


Figure 3. Spatial distribution of the dominant (1a–1f) and second most dominant (2a–2f) AR–weather system combinations across AR scales. Colors indicate the most frequent combination at each grid cell, while shading represents the frequency of occurrence, with lighter shades indicating lower frequency and darker hues indicating higher frequency. The circular legends on the right show the categorical color mapping and representative frequency scale for the dominant (top) and second most dominant (bottom) combinations, respectively.

3.3. Spatial Patterns of Dominant AR Co-Occurrences

To assess regional variations in AR co-occurrence, we analyze spatial patterns of co-occurring systems across grid cells. Figure 3 shows the dominant and second-most dominant co-occurring systems for the annual aggregate and for each AR scale. For the annual aggregate across all scales (Figure 3-1a), AR + Front combinations are the most dominant along the western U.S. coast. Inland regions show greater variability, with some areas, such as those surrounding the Rockies, characterized by patchy AR-only occurrences before transitioning back to AR + Front combinations across the Midwest and eastern U.S. In the southeastern U.S., ARs frequently co-occur with LPS or with combined AR + MCS + LPS configurations, although AR-only occurrences become more common north of the Gulf of Mexico.

Patterns for scales 1–3 (Figures 3-1b–3-1d) largely resemble the annual distribution (Figure 3-1a). AR + Front combinations dominate most regions, including the West, Southeast, East, and Midwest, while AR-only occurrences appear in some inland areas. In the higher scales (3–4; Figures 3-1d and 3-1e), increased occurrences of AR + MCS and AR + Front + MCS combinations appear offshore of western North America in the Pacific, a region of frequent AR genesis that has been linked to some of the costliest ARs impacting the western U.S. (Prince et al., 2021). This offshore enhancement likely reflects synoptic environments associated with extratropical cyclones, characterized by stronger frontal organization and enhanced horizontal moisture transport (Neiman et al., 2008; Ralph et al., 2004, 2005, 2006; Wernli & Davies, 1997). Such conditions likely explain the frequent AR + Front co-occurrence observed in lower AR scales (Bao et al., 2006; Zhang et al., 2019). By AR scale 5, a shift occurs over the eastern Pacific and offshore of northwestern Mexico, where AR + LPS combinations become more prevalent. This pattern may reflect the co-occurrence of high AR scales with tropical or

19448007, 2026, 18, Downloaded from https://agupubs.onlinelibrary.wiley.com/doi/10.1029/2026GL123975, Wiley Online Library on [03/11/2026]. See the Terms and Conditions (https://onlinelibrary.wiley.com/terms-and-conditions) on Wiley Online Library for rules of use; OA articles are governed by the applicable Creative Commons License

19448007, 2026, 18, Downloaded from https://agupubs.onlinelibrary.wiley.com/doi/10.1029/2026GL123975, Wiley Online Library on [03/11/2026]. See the Terms and Conditions (https://onlinelibrary.wiley.com/terms-and-conditions) on Wiley Online Library for rules of use; OA articles are governed by the applicable Creative Commons License

transitioning cyclones, which are most active from late spring through autumn and peak in late August or early September (Larson et al., 2005).

These patterns are also reflected in the second-most dominant configurations (Figures 3-2a–3-2f). Along much of the western U.S. coast, as well as across parts of the Midwest and northeastern U.S., AR + Front + MCS combinations frequently appear as the second-most dominant pattern. In contrast, the southern portion of the western U.S. coast and the adjacent Pacific region show more AR-only grid cells in the lowest scales (1–2). As AR scale increases, these areas exhibit more frequent MCS-related combinations, particularly AR + MCS and AR + Front + MCS. Similar to the most dominant pattern in AR scale 5, LPS-related configurations also become more common in these offshore Pacific regions in the second-most dominant scenario, in some areas in combination with AR + Front.

The Gulf of Mexico region in Figures 3-1a–3-1f exhibits a different evolution across AR scales. In the lowest scales (1–2), AR + Front combinations dominate, while AR-only occurrences are also common. Beginning in AR scale 3, the dominant patterns become more heterogeneous, with increased occurrences of AR-only, AR + LPS, AR + MCS, and, in some areas, AR + MCS + LPS combinations. The second-most dominant configurations in this region commonly include AR + Front and, in localized areas, AR + MCS + LPS. By scales 4–5, the Gulf region shows a broader mix of AR-, LPS-, and MCS-related combinations, with similar diversity also appearing in the second-most dominant patterns (Figure 3-2a–3-2f), though generally at lower frequency.

Taken together, the dominant and second-most dominant spatial patterns suggest that the contrasting AR archetypes illustrated in Figure 1 occur with varying prominence across the U.S. The canonical midlatitude regime, characterized by strong AR–front co-occurrence, remains dominant across much of the western, midwestern, and northeastern U.S., and is also frequently present in the Gulf region. However, in the Gulf and Pacific genesis regions, higher AR scales exhibit greater complexity through more frequent co-occurrence with MCSs and LPSs.

4. Discussion

Previous studies highlight the range of dynamical structures associated with ARs, from canonical synoptic-scale frontal systems to more complex interactions with embedded convective and cyclonic features. The dominance of AR–Front co-occurrence in our results is consistent with previous studies showing that ARs are frequently embedded within synoptic-scale flow and frontal structures (Ralph et al., 2004, 2005, 2006; Bao et al., 2006; Neiman et al., 2008; H. F. Dacre et al., 2019). Our findings further suggest that while this canonical frontal regime remains dominant across seasons, regions, and AR scales, higher AR scales exhibit increasing complexity through more frequent co-occurrence with MCSs and LPSs. These stronger AR events may also be associated with enhanced low-level jets, warm advection, and more organized moisture transport structures (Cobb et al., 2021; Hu & Dominguez, 2019). Together, these findings indicate that AR development arises from multiple interacting mechanisms. Our co-occurrence analysis over the U.S. is consistent with this framework and further suggests that the prevalence of co-occurring systems varies systematically by region and AR scale.

Across much of the CONUS, AR–Front interactions dominate, reflecting the influence of large-scale synoptic systems in organizing moisture transport, particularly during DJF and MAM when extratropical cyclone activity peaks (Bao et al., 2006; Zhang et al., 2019). In contrast, regions in the lower extratropics, such as the Gulf Coast, exhibit increasing contributions from LPSs and MCSs, especially in higher AR scales and during JJA and SON. This pattern suggests that secondary moisture transport pathways and convective processes more frequently co-occur with ARs, consistent with the seasonal peaks in LPS and MCS activity (Ashley et al., 2003; Larson et al., 2005; Slinskey et al., 2020). The warm-season westward extension of the North Atlantic Subtropical High may further enhance Gulf moisture transport, creating conditions favorable for MCS and LPS activity (W. Li et al., 2011; L. Li et al., 2018). Differences in MCS behavior between spring (synoptically driven) and summer (mesoscale-driven) further support the reduced role of frontal forcing and the increased importance of convection in shaping AR-related moisture transport (Song et al., 2019).

To summarize how these co-occurrence patterns relate to precipitation, Figure 4 presents the fraction of precipitation contributed by each co-occurrence type across AR scales across over the North American study domain (0°–60°N, 160°–50°W). At the annual scale, as AR scale increases, the fractional contribution from AR + Front interactions modestly decreases (particularly from AR scales 3–5), while precipitation associated with a broader range of co-occurrence patterns becomes more prominent (although AR-Front-MCS contributions remain

10.1029/2026GL123975

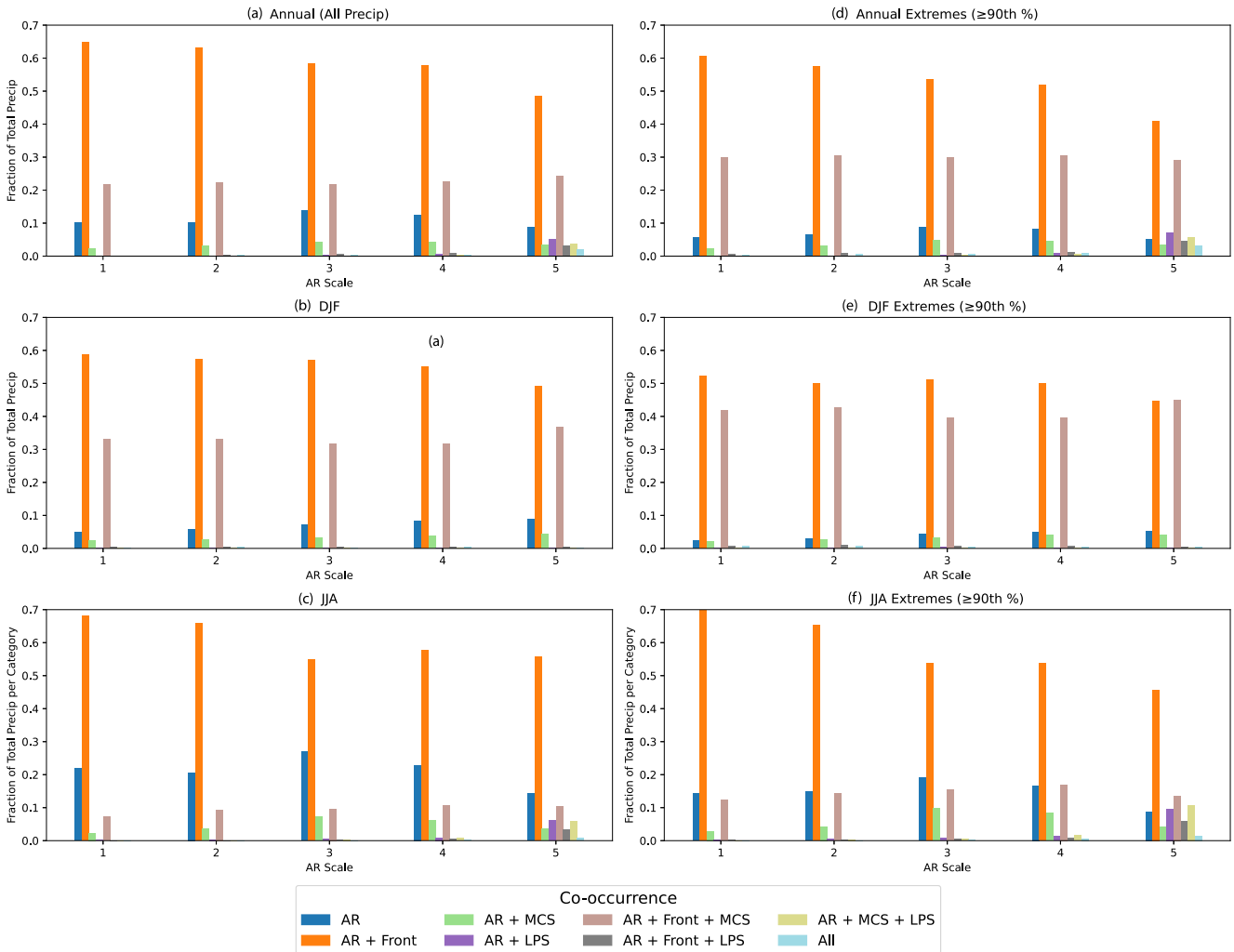


Figure 4. Fraction of precipitation associated with different co-occurring systems during AR events across AR scales. Panels (a–c) show the annual distribution and seasonal distributions for DJF and JJA. Panels (d–f) show the corresponding precipitation distributions exceeding the 90th percentile for each scale. For each scale, the total fractional precipitation sums to 1.

relatively constant with AR scale). Across extreme precipitation scenarios, AR + Front remains the dominant baseline configuration; however, AR + Front + MCS combinations become substantially more prominent compared to the annual mean case. This signal is especially pronounced in DJF, where AR + Front + MCS contributes a much larger fraction of precipitation during extreme events than during all precipitation events.

Seasonal differences are also evident. DJF presents a comparatively simpler structure, where co-occurrences are primarily limited to AR, Front, and MCS combinations. Under extreme precipitation conditions, AR + Front + MCS events contribute nearly the same fraction as AR + Front events alone, highlighting the importance of frontal forcing and embedded convection in cool-season AR precipitation.

During JJA, while AR + Front combinations continue to provide the dominant contribution, AR-only grid cells exhibit a relatively larger fractional contribution. During extreme precipitation events, AR + Front + MCS combinations and AR-only points contribute similarly, roughly 10%–15% each, indicating a greater prevalence of convective-related co-occurrences in higher-intensity AR precipitation events. In AR scale 5, LPS-related co-occurrences show increased precipitation contributions (totaling over 20% of grid cells), which are further enhanced under extreme conditions. The emergence of AR, front, MCS and LPS combinations at the highest AR scales suggests that the most intense warm-season AR events occur in environments where frontal, convective, and cyclonic processes interact.

19448007, 2026, 18, Downloaded from https://agupubs.onlinelibrary.wiley.com/doi/10.1029/2026GL123975, Wiley Online Library on [03/11/2026]. See the Terms and Conditions (https://onlinelibrary.wiley.com/terms-and-conditions) on Wiley Online Library for rules of use; OA articles are governed by the applicable Creative Commons License

19448007, 2026, 18, Downloaded from https://agupubs.onlinelibrary.wiley.com/doi/10.1029/2026GL123975, Wiley Online Library on [03/11/2026]. See the Terms and Conditions (https://onlinelibrary.wiley.com/terms-and-conditions) on Wiley Online Library for rules of use; OA articles are governed by the applicable Creative Commons License

Although AR–Front interactions dominate off the U.S. West Coast, Figure 3 also indicates the presence of MCS activity associated with these events. Large MCSs develop over the Pacific warm pool and play a fundamental role in intraseasonal and interannual climate variability (Chen et al., 1996; Nakazawa, 1988). Additionally, LPS activity in the Gulf region exhibits intraseasonal and interannual variability, and may modulate moisture transport pathways (Landsea, 1993). Together, these processes may contribute to seasonal and regional variability in AR-related precipitation.

Overall, these results indicate that stronger ARs are associated with increasingly complex co-occurrence structures involving multiple interacting weather systems. The seasonal patterns suggest that intense ARs can emerge through both large-scale synoptic moisture transport and interactions with smaller-scale mesoscale and transient systems that modulate AR variability (Kamnani et al., 2025). From a forecasting perspective, the simultaneous presence of ARs with other synoptic and mesoscale features, particularly fronts, MCSs, and LPSs, may indicate the potential for higher AR scale events and associated extreme precipitation.

These findings highlight the importance of considering multi-system interactions in AR analysis. While this study quantifies the frequency and spatial distribution of co-occurring weather systems, it does not explicitly evaluate the dynamical interactions through which ARs, fronts, MCSs, and LPSs may strengthen or modify one another. Previous studies have shown that interactions among a subset of these systems can influence moisture transport, precipitation characteristics, and event evolution (H. F. Dacre et al., 2019; K. T. Quagraine et al., 2026; Zhang et al., 2019). Future work could therefore investigate how such interactions affect AR intensity, precipitation generation, and associated hydrological and societal impacts.

5. Conclusion

In summary, this study shows that ARs across different scales in the U.S. are associated with a diverse set of interacting weather systems whose relative importance depends on both season and region. Across much of the conterminous U.S., ARs are most commonly linked with frontal systems, consistent with the classical midlatitude configuration in which ARs are embedded within the extratropical cyclones. However, stronger AR events increasingly exhibit more complex structures involving MCSs and LPSs. This complexity is most evident during winter and spring through enhanced convective co-occurrence, and during summer and autumn through the more frequent presence of both convective and cyclonic systems, particularly in the Gulf Coast and Pacific genesis regions. As AR scale increases, these interacting structures become more varied, reflecting the combined influence of multiple weather systems. During extreme precipitation events, convective-related contributions become especially pronounced in DJF, whereas in JJA higher-scale events are associated with a broader range of co-occurrence patterns. Recognizing these regionally and seasonally varying configurations provides important context for interpreting AR-related precipitation extremes and suggests that the simultaneous presence of ARs with fronts, MCSs, and LPSs may serve as a useful indicator of potential high-impact events.

Conflict of Interest

The authors declare no conflicts of interest relevant to this study.

Availability Statement

The 19-year integrated feature-precipitation data set, provided at 6-hourly resolution, can be accessed at Dryad (Tsai et al., 2024). Atmospheric River categorization were conducted using the ARCat Python toolkit (K. Quagraine, 2024). Atmospheric River identification software can be obtained from TECA-BARD (Loring et al., 2020). ERA5 reanalysis data, can be accessed through the National Center for Atmospheric Research Research Data Archive (European Centre for Medium-Range Weather Forecasts, 2019). The codes and figures for this analysis are available at (Kamnani, 2026).

Acknowledgments
This material is based upon work supported by the Director, Office of Science, Office of Biological and Environmental Research of the U.S. Department of Energy under Contract No. DE-AC02-05CH11231 and by the Regional and Global Model Analysis Program area within the Earth and Environmental Systems Modeling Program (under Contract Nos. DE-SC0023244 and DE-SC0023519). The research used resources of the National Energy Research Scientific Computing Center (NERSC), also supported by the Office of Science of the U.S. Department of Energy, under Contract No. DE-AC02-05CH11231. This research was supported in part by Lilly Endowment, Inc., through its support for the Indiana University Pervasive Technology Institute. The Pacific Northwest National Laboratory is operated for Department of Energy by Battelle Memorial Institute under contract DE-AC05-76RL01830. We acknowledge Samuel Smith and Christine Shields for their valuable insights and discussions during the development of this research.

References

Algarra, I., Eiras-Barca, J., Miguez-Macho, G., Nieto, R., & Gimeno, L. (2019). On the assessment of the moisture transport by the Great Plains low-level jet. *Earth System Dynamics*, *10*(1), 107–119. https://doi.org/10.5194/esd-10-107-2019

Ashley, W. S., Mote, T. L., Dixon, P. G., Trotter, S. L., Powell, E. J., Durkee, J. D., & Grundstein, A. J. (2003). Distribution of mesoscale convective complex rainfall in the United States. *Monthly Weather Review*, *131*(12), 3003–3017. https://doi.org/10.1175/1520-0493(2003)131<3003:domccr>2.0.co;2

Bao, J.-W., Michelson, S. A., Neiman, P. J., Ralph, F. M., & Wilczak, J. M. (2006). Interpretation of enhanced integrated water vapor bands associated with extratropical cyclones: Their formation and connection to tropical moisture. *Monthly Weather Review*, *134*(4), 1063–1080. https://doi.org/10.1175/MWR3123.1

Bjerknes, J., & Solberg, H. (1922). Life cycle of cyclones and the polar front theory of atmospheric circulation. *Geofysiske Publikasjoner*, *3*(1), 3–18. https://journals.ametsoc.org/view/journals/mwre/50/9/1520-0493_1922_50_468_jbahso_2_0_co_2.xml

Catto, J. L., & Dowdy, A. (2021). Understanding compound hazards from a weather system perspective. *Weather and Climate Extremes*, *32*, 100313. https://doi.org/10.1016/j.wace.2021.100313

Chen, S. S., Houze, R. A., & Mapes, B. E. (1996). Multiscale variability of deep convection in realation to large-scale circulation in TOGA COARE. *Journal of the Atmospheric Sciences*, *53*(10), 13. https://doi.org/10.1175/1520-0469(1996)053<1380:mvodci>2.0.co;2

Cobb, A., Michaelis, A., Iacobellis, S., Ralph, F. M., & Monache, L. D. (2021). Atmospheric river sectors: Definition and characteristics observed using dropsondes from 2014–20 CalWater and AR recon. *Monthly Weather Review*, *149*(3), 623–644. https://doi.org/10.1175/MWR-D-20-0177.1

Cordeira, J. M., Ralph, F. M., & Moore, B. J. (2013). The development and evolution of two atmospheric Rivers in proximity to Western north Pacific tropical cyclones in October 2010. *Monthly Weather Review*, *141*(12), 23. https://doi.org/10.1175/MWR-D-13-00019.1

Corringham, T. W., Ralph, F. M., Gershunov, A., Cayan, D. R., & Talbot, C. A. (2019). Atmospheric Rivers drive flood damages in the western United States. *Science Advances*, *5*(12), eaax4631. https://doi.org/10.1126/sciadv.aax4631

Dacre, H. (2020). A review of extratropical cyclones: Observations and conceptual models over the past 100 years. *Weather*, *75*(1), 4–7. https://doi.org/10.1002/wea.3653

Dacre, H. F., Martínez-Alvarado, O., & Mbengue, C. O. (2019). Linking atmospheric Rivers and warm conveyor belt airflows. *Journal of Hydrometeorology*, *20*(6), 1183–1196. https://doi.org/10.1175/JHM-D-18-0175.1

European Centre for Medium-Range Weather Forecasts. (2019). ERA5 reanalysis (0.25 degree latitude-longitude grid) [Dataset]. *NSF National Center for Atmospheric Research*. Retrieved from https://gdex.ucar.edu.doi:10.5065/BH6N-5N20

Feng, Z., Hardin, J., Barnes, H. C., Li, J., Leung, L. R., Varble, A., & Zhang, Z. (2023). PyFLEXTRKR: A flexible feature tracking python software for convective cloud analysis. *Geoscientific Model Development*, *16*(10), 2753–2776. https://gmd.copernicus.org/articles/16/2753/2023/doi:10.5194/gmd-16-2753-2023

Gimeno, L., Dominguez, F., Nieto, R., Trigo, R., Drumond, A., Reason, C. J. C., et al. (2016). Major mechanisms of atmospheric moisture transport and their role in extreme precipitation events. *Annual Review of Environment and Resources*, *41*(1), 117–141. https://doi.org/10.1146/annurev-environ-110615-085558

Gimeno, L., Vázquez, M., Eiras-Barca, J., Sorí, R., Stojanovic, M., Algarra, I., et al. (2020). Recent progress on the sources of continental precipitation as revealed by moisture transport analysis. *Earth-Science Reviews*, *201*, 103070. https://doi.org/10.1016/j.earscirev.2019.103070

Hersbach, H., Bell, B., Berrisford, P., Hirahara, S., Horányi, A., Muñoz-Sabater, J., et al. (2020). The ERA5 global reanalysis. *Quarterly Journal of the Royal Meteorological Society*, *146*(730), 1999–2049. https://doi.org/10.1002/qj.3803

Hsu, H.-H., & Chen, Y.-T. (2020). Simulation and projection of circulations associated with atmospheric Rivers along the north American Northeast Coast. *Journal of Climate*, *33*(13), 5673–5695. https://doi.org/10.1175/JCLI-D-19-0104.1

Hu, H., & Dominguez, F. (2019). Understanding the role of tropical moisture in atmospheric Rivers. *Journal of Geophysical Research: Atmospheres*, *124*(24), 13826–13842. https://doi.org/10.1029/2019JD030867

Huffman, G. J., Bolvin, D. T., Braithwaite, D., Hsu, K., Joyce, R., Xie, P., & Yoo, S.-H. (2015). NASA global precipitation measurement (GPM) integrated multi-satellite retrievals for GPM (IMERG). *Algorithm theoretical basis document (ATBD) version*, *4*(26), 30.

Janowiak, J. E., Joyce, R. J., & Yarosh, Y. (2001). A real-time global half-hourly pixel-resolution infrared dataset and its applications. *Bulletin of the American Meteorological Society*, *82*(2), 205–218. https://doi.org/10.1175/1520-0477(2001)082<0205:artghh>2.3.co;2

Kamnani, D. (2026). Analysis codes and figures for Co-Occurring weather systems vary by atmospheric river scale across the United States [Software]. *Zenodo*. https://doi.org/10.5281/zenodo.20693669

Kamnani, D., O'Brien, T. A., Smith, S., Staten, P. W., & Shields, C. A. (2025). Regional and temporal variability of atmospheric river seasonality: Influences of detection algorithms and moisture transport dynamics. *Journal of Geophysical Research: Atmospheres*, *130*(14), e2024JD043032. https://doi.org/10.1029/2024JD043032

Landsea, C. W. (1993). A climatology of intense (or major) Atlantic hurricanes. *Monthly Weather Review*, *121*(6), 1703–1713. https://doi.org/10.1175/1520-0493(1993)121⟨1703:ACOIMA⟩2.0.CO;2

Larson, J., Zhou, Y., & Higgins, R. W. (2005). Characteristics of landfalling tropical cyclones in the United States and Mexico: Climatology and interannual variability. *Journal of Climate*, *18*(8), 1247–1262. https://doi.org/10.1175/JCLI3317.1

Lavers, D. A., & Villarini, G. (2013). Atmospheric Rivers and flooding over the central United States. *Journal of Climate*, *26*(20), 7829–7836. https://doi.org/10.1175/JCLI-D-13-00212.1

Li, L., Li, W., & Deng, Y. (2018). Summer rainfall variability over the Southeastern United States and its intensification in the 21st century as assessed by CMIP5 models. *Journal of Geophysical Research: Atmospheres*, *118*(2), 340–354. https://doi.org/10.1002/jgrd.50136

Li, W., Li, L., Fu, R., Deng, Y., & Wang, H. (2011). Changes to the North Atlantic subtropical high and its role in the intensification of summer rainfall variability in the Southeastern United States. *Journal of Climate*, *24*(5), 1499–1506. https://doi.org/10.1175/2010JCLI3829.1

Loring, B., O'Brien, T. A., Elbashandy, A. E., Johnson, J. N., Krishnan, H., Keen, N., et al. (2020). Toolkit for extreme climate analysis - TECA bayesian AR detector v1.0.1 [Software]. *Zenodo*. https://doi.org/10.5281/zenodo.4130468

Mahoney, K., Jackson, D. L., Neiman, P., Abel, M. R., Darby, L., Wick, G., et al. (2016). Understanding the role of atmospheric Rivers in heavy precipitation in the Southeast United States. *Monthly Weather Review*, *144*(4), 1617–1632. https://doi.org/10.1175/MWR-D-15-0279.1

Moore, B. J., Neiman, P. J., Ralph, F. M., & Barthold, F. E. (2012). Physical processes associated with heavy flooding rainfall in Nashville, Tennessee, and vicinity during 1–2 May 2010: The role of an atmospheric River and mesoscale convective systems. *Monthly Weather Review*, *140*(2), 358–378. https://doi.org/10.1175/MWR-D-11-00126.1

Nakazawa, T. (1988). Tropical super clusters within intraseasonal variations over the Western Pacific. *Journal of the Meteorological Society of Japan. Ser. II*, *66*(6), 823–839. https://doi.org/10.2151/jmsj1965.66.6_823

Neiman, P. J., Ralph, F. M., Wick, G. A., Lundquist, J. D., & Dettinger, M. D. (2008). Meteorological characteristics and overland precipitation impacts of atmospheric Rivers affecting the West Coast of North America based on eight years of SSM/I satellite observations. *Journal of Hydrometeorology*, *9*(1), 22–47. https://doi.org/10.1175/2007JHM855.1

Newell, R. E., & Zhu, Y. (1994). Tropospheric rivers: A one-year record and a possible application to ice core data. *Geophysical Research Letters*, *21*(2), 113–116. https://doi.org/10.1029/93GL03113

O'Brien, T. A., Loring, B., Dufek, A. S., Islam, M. R., Kamnani, D., Quagraine, K. T., & Kirkpatrick, C. (2024). Atmospheric Rivers in the Eastern and midwestern United States associated with baroclinic waves. *Geophysical Research Letters*, *51*(8), e2023GL107236. https://doi.org/10.1029/2023GL107236

19448007, 2026, 18, Downloaded from https://agupubs.onlinelibrary.wiley.com/doi/10.1029/2026GL123975, Wiley Online Library on [03/11/2026]. See the Terms and Conditions (https://onlinelibrary.wiley.com/terms-and-conditions) on Wiley Online Library for rules of use; OA articles are governed by the applicable Creative Commons License

O'Brien, T. A., Wehner, M. F., Payne, A. E., Shields, C. A., Rutz, J. J., Leung, L.-R., et al. (2022). Increases in future AR count and size: Overview of the ARTMIP tier 2 CMIP5/6 experiment. *Journal of Geophysical Research: Atmospheres*, *127*(6), e2021JD036013. https://doi.org/10.1029/2021JD036013

Pradhan, S., Wasko, C., & Peel, M. C. (2026). Atmospheric rivers increase global flood risk. *Environmental Research Letters*, *21*(2), 024013. https://doi.org/10.1088/1748-9326/ae362a

Prein, A. F., Mooney, P. A., & Done, J. M. (2023). The multi-scale interactions of atmospheric phenomenon in mean and extreme precipitation. *Earth's Future*, *11*(11), e2023EF003534. https://doi.org/10.1029/2023EF003534

Prince, H. D., Gibson, P. B., DeFlorio, M. J., Corringham, T. W., Cobb, A., Guan, B., et al. (2021). Genesis locations of the costliest atmospheric Rivers impacting the Western United States. *Geophysical Research Letters*, *48*(20), e2021GL093947. https://doi.org/10.1029/2021GL093947

Quagraine, K. (2024). ARCat: Atmospheric river categorization toolkit [Software]. https://pypi.org/project/arcat/

Quagraine, K. T., O'Brien, T. A., Boos, W., Neelin, J. D., Tsai, W.-M., Leung, L. R., et al. (2026). Compound mesoscale convective systems and low-pressure systems in tropical monsoon regions: Assessing their meteorology and precipitation. *Journal of Geophysical Research: Atmospheres*, *131*(10), e2025JD046151. https://doi.org/10.1029/2025JD046151

Quagraine, K. T., O'Brien, T. A., & Zhou, Y. (2025). Similarities in meteorological composites among different atmospheric river detection tools during landfall over Western coastal North America. *Journal of Geophysical Research: Atmospheres*, *130*(6), e2024JD042163. https://doi.org/10.1029/2024JD042163

Ralph, F. M., Neiman, P. J., & Rotunno, R. (2005). Dropsonde observations in low-level jets over the northeastern Pacific Ocean from CALJET-1998 and PACJET-2001: Mean vertical-profile and atmospheric-river characteristics. *Monthly Weather Review*, *133*(4), 889–910. https://doi.org/10.1175/MWR2896.1

Ralph, F. M., Neiman, P. J., & Wick, G. A. (2004). Satellite and CALJET aircraft observations of atmospheric Rivers over the eastern north Pacific Ocean during the winter of 1997/98. *Monthly Weather Review*, *132*(7), 1721–1745. https://doi.org/10.1175/1520-0493(2004)132<1721:sacaoo>2.0.co;2

Ralph, F. M., Neiman, P. J., Wick, G. A., Gutman, S. I., Dettinger, M. D., Cayan, D. R., & White, A. B. (2006). Flooding on California's Russian river: Role of atmospheric rivers. *Geophysical Research Letters*, *33*(13). https://doi.org/10.1029/2006GL026689

Ralph, F. M., Rutz, J. J., Cordeira, J. M., Dettinger, M., Anderson, M., Reynolds, D., et al. (2019). A scale to characterize the strength and impacts of atmospheric Rivers. *Bulletin of the American Meteorological Society*, *100*(2), 269–289. https://doi.org/10.1175/BAMS-D-18-0023.1

Sansom, P. G., & Catto, J. L. (2024). Objective identification of meteorological fronts and climatologies from ERA-interim and ERA5. *Geoscientific Model Development*, *17*(16), 6137–6151. https://doi.org/10.5194/gmd-17-6137-2024

Slinskey, E. A., Loikith, P. C., Waliser, D. E., Guan, B., & Martin, A. (2020). A climatology of atmospheric Rivers and associated precipitation for the seven U.S. national climate assessment regions. *Journal of Hydrometeorology*, *21*(11). https://doi.org/10.1175/JHM-D-20-0039.1

Song, F., Feng, Z., Leung, L. R., Jr, R. A. H., Wang, J., Hardin, J., & Homeyer, C. R. (2019). Contrasting spring and summer large-scale environments associated with mesoscale convective systems over the U.S. Great Plains. *Journal of Climate*, *32*(20), 6749–6767. https://doi.org/10.1175/JCLI-D-18-0839.1

Tsai, W.-M., Duan, S., O'Brien, T. A., Catto, J. L., Ullrich, P. A., Zhou, Y., et al. (2025). Co-Occurring atmospheric features and their contributions to precipitation extremes. *Journal of Geophysical Research: Atmospheres*, *130*(5), e2024JD041687. https://doi.org/10.1029/2024JD041687

Tsai, W.-M., O'Brien, T., Catto, J., Ullrich, P., Leung, L.-Y., Fang, Z., et al. (2024). Precipitation identifiers for meteorological features combining global GPM-IMERG retrievals and ERA5 reanalysis [Dataset]. *Dryad*. https://doi.org/10.5061/DRYAD.V9S4MW73G

Vishnu, S., Boos, W. R., Ullrich, P. A., & O'Brien, T. A. (2020). Global track dataset of monsoon low pressure systems. *Zenodo*. https://doi.org/10.5281/zenodo.3890646

Wakefield, R. A., Basara, J. B., Shepherd, J. M., Brauer, N., Furtado, J. C., Jr, J. A. S., & Edwards, R. (2021). The Inland maintenance and reintensification of tropical storm bill (2015). Part I: Contributions of the brown ocean effect. *Journal of Hydrometeorology*, *22*(10), 2675–2693. https://doi.org/10.1175/JHM-D-20-0150.1

Wernli, H., & Davies, H. C. (1997). A Lagrangian-based analysis of extratropical cyclones. I: The method and some applications. *Quarterly Journal of the Royal Meteorological Society*, *123*(538), 467–489. https://doi.org/10.1002/qj.49712353811

Zhang, Z., Ralph, F. M., & Zheng, M. (2019). The relationship between extratropical cyclone strength and atmospheric river intensity and position. *Geophysical Research Letters*, *46*(3), 1814–1823. https://doi.org/10.1029/2018GL079071

19448007, 2026, 18, Downloaded from https://agupubs.onlinelibrary.wiley.com/doi/10.1029/2026GL123975, Wiley Online Library on [03/11/2026]. See the Terms and Conditions (https://onlinelibrary.wiley.com/terms-and-conditions) on Wiley Online Library for rules of use; OA articles are governed by the applicable Creative Commons License